Automatic insertion of simulated microcalcification clusters in a software breast phantom

Varsha Shankla*, David D. Pokrajac[a], Susan P. Weinstein, Michael DeLeo,
Catherine Tuite, Robyn Roth, Emily F. Conant, Andrew D.A. Maidment, Predrag R. Bakic
Department of Radiology, University of Pennsylvania, Philadelphia, PA
[a]Computer and Information Sciences Department, Delaware State University, Dover, DE

ABSTRACT

An automated method has been developed to insert realistic clusters of simulated microcalcifications (MCs) into computer models of breast anatomy. This algorithm has been developed as part of a virtual clinical trial (VCT) software pipeline, which includes the simulation of breast anatomy, mechanical compression, image acquisition, image processing, display and interpretation. An automated insertion method has value in VCTs involving large numbers of images. The insertion method was designed to support various insertion placement strategies, governed by probability distribution functions (pdf). The pdf can be predicated on histological or biological models of tumor growth, or estimated from the locations of actual calcification clusters. To validate the automated insertion method, a 2-AFC observer study was designed to compare two placement strategies, undirected and directed. The undirected strategy could place a MC cluster anywhere within the phantom volume. The directed strategy placed MC clusters within fibroglandular tissue on the assumption that calcifications originate from epithelial breast tissue. Three radiologists were asked to select between two simulated phantom images, one from each placement strategy. Furthermore, questions were posed to probe the rationale behind the observer's selection. The radiologists found the resulting cluster placement to be realistic in 92% of cases, validating the automated insertion method. There was a significant preference for the cluster to be positioned on a background of adipose or mixed adipose/fibroglandular tissues. Based upon these results, this automated lesion placement method will be included in our VCT simulation pipeline.

Keywords: Software breast phantom, simulated microcalcification clusters, volumetric distribution of breast microcalcifications, 2-AFC observer study

1. INTRODUCTION

A variety of new 3D breast imaging technologies (e.g., stereomammography, tomosynthesis and computed tomography) are currently undergoing clinical investigation. These modalities offer specific technical advantages, such as superior spatial or contrast resolution. However, before widespread clinical adoption can occur, any new breast imaging system must undergo optimization and pass clinical validation. To safely accelerate this process, we have developed a preclinical validation method in the form of virtual clinical trials (VCT), based upon computer simulations of breast anatomy, image acquisition and interpretation (1-4). Other simulations of breast imaging have also been reported (5-9). Breast anatomy simulation provides the flexibility needed to simulate a broad range of anatomical variations, while providing the ground truth of simulated tissues needed for quantitative validation.

The visibility of microcalcification (MCs) in clinical images is of critical importance for breast imaging, as MCs can be the only sign of early cancer. To conduct a VCT of early breast cancer screening comparing digital mammography (DM) and digital breast tomosynthesis (DBT), we developed a method to insert MC clusters into our existing breast anatomy model automatically. Simulation of MC clusters in breast images has been reported in the literature. MC clusters have been extracted from both biopsy specimen (10, 11) or mastectomy specimen (12) images. Here, we report on a method using clusters extracted from stereoscopic biopsy images (13, 14).

Previous reports used manually selected locations (11). Here, we implement two automated strategies for MC placement: "undirected" and "directed". Both strategies use an underlying probability distribution function (PDF) of potential cluster locations. In the undirected strategy, the PDF is uniform within the entire volume of the breast, while in

* VarshaSh@seas.upenn.edu, DPokrajac@desu.edu, [Susan.Weinstein | Michael.DeLeo | Catherine.Tuite | Robyn.Gartner | Emily.Conant | Andrew.Maidment | Predrag.Bakic]@uphs.upenn.edu

Medical Imaging 2014: Physics of Medical Imaging, edited by Bruce R. Whiting, Christoph Hoeschen, Despina Kontos,
Proc. of SPIE Vol. 9033, 90331Z · © 2014 SPIE · CCC code: 1605-7422/14/$18 · doi: 10.1117/12.2044337

the directed strategy, the PDF is based upon the breast anatomy. In this paper, we consider a directed strategy in which MC only occur within fibroglandular tissue regions. The insertion method and placement strategies were validated in a two-alternative forced-choice (2-AFC) observer study with three radiologist observers.

2. MATERIALS AND METHODS

2.1 Breast anatomy simulation

2.2.1 Simulation of normal breast tissue

The Penn anthropomorphic software phantom simulates the breast as a set of tissues arrayed spatially, including: skin, adipose tissue, fibroglandular tissue, and Cooper's ligaments. Compartments within a matrix of Cooper's ligaments are simulated using a recursive partitioning algorithm (4). The compartments are then filled with adipose or glandular tissue according to rules governing spatial distribution (15). The resulting compartments vary in shape and size, creating a realistic simulation of the breast parenchyma. Simulation parameters can be set to simulate the full breadth of breast anatomy observed clinically.

After the generation of the breast phantom, clinical mammographic compression of the phantom is modeled by deforming the uncompressed phantom using 3D finite element methods (16-18). Mammography and DBT image acquisition is currently simulated by ray tracing projections through the phantom, as described below. Processed DM and reconstructed DBT images are obtained using the Real-Time Tomography (RTT, Villanova, PA) image processing and reconstruction software (19).

2.1.2 Simulation of calcification clusters

MC clusters used in this work are from an existing database of 130 clusters segmented from anonymized stereoscopic breast biopsy images (13, 14). Each cluster in the database is stored as a 3D binary volume, with a voxel value of '1' representing calcified material and a value of '0' representing the background tissue. Before insertion, each cluster is resampled to match the phantom voxel size. Since the clusters are most typically down-sampled, a fractional volume per voxel is calculated to preserve the quality of the MCs. Fig. 1 illustrates a selection of simulated MC clusters; the images were created by 3D rendering tomographic images in an orientation identical to that used in the study. Fig. 2 provides additional details regarding the 130 clusters available in the database. A histogram of the volume of individual MCs in shown in Fig. 2A; a histogram of the cluster volume is shown in Fig. 2B; and, a histogram of the number of MCs in a cluster is shown in Fig. 2C. These data show that the MCs and clusters used in the study are representative of those seen clinically.

(a) (b) (c)

Figure 1: 3D renderings of simulated clusters corresponding to (a) a benign fibroadenoma; (b) malignant DCIS (micropapillary grade 1); and (c) benign fibrocystic change with focal sclerosing adenosis.

2.2 Cluster insertion method

A flowchart of the automatic insertion method is shown in Fig. 3. The process begins with the selection of a phantom and a cluster to be inserted. A volume of interest (VOI) within the breast is determined based upon the probability distribution function of potential cluster locations. The software then searches for potential locations within the VOI. First, the minimum rectangular hull of the cluster (a rectangular prism that envelopes the cluster) is calculated. Then, the rectangular hull is convolved with the VOI to generate a set of candidate locations. The convolution is performed sequentially along the three orthogonal axes for computational expediency. The software then randomly selects one of

the candidate locations as the point of insertion. If the convolution does not return any candidate insertion points, then that phantom cannot be used with that cluster.

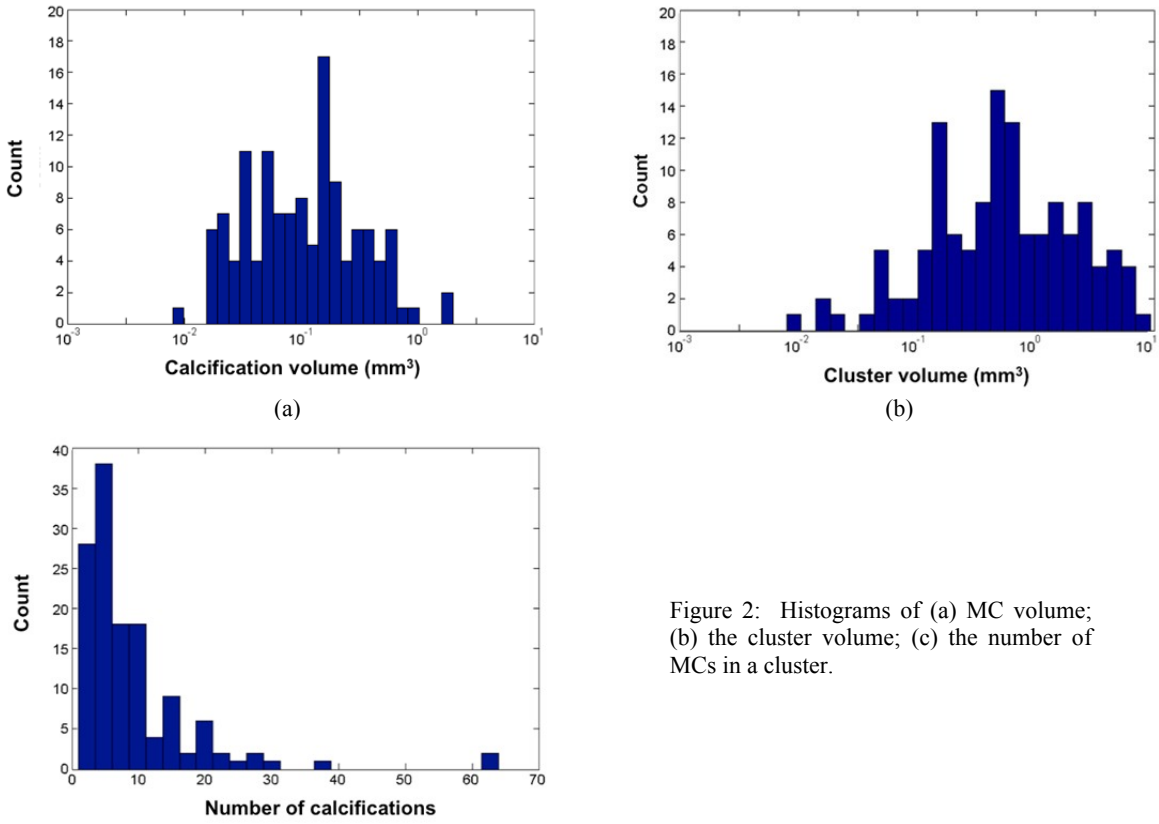

Figure 2: Histograms of (a) MC volume; (b) the cluster volume; (c) the number of MCs in a cluster.

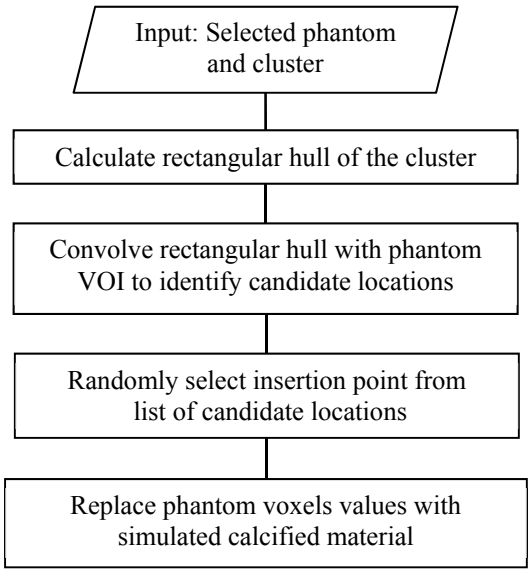

Figure 3: Flowchart of the automatic insertion process

A cluster is inserted into a phantom by replacing the voxel values of the phantom with calcified material (as detailed below) wherever the binary value of the cluster model is "1". In this work, the orientation of the cluster from the original database is preserved during insertion. Rotation of the cluster model would require recalculation of the rectangular hull. Rotation is one of the methods we intend to explore in the future to increase the variability of the cluster appearance.

We have evaluated both directed and undirected MC cluster placement strategies. The undirected strategy assumes that MCs can be located anywhere within the breast volume. The directed strategy assumes that the location of MCs is restricted in some sense. Here we implement a directed strategy based upon the assumption that MC clusters of clinical interest are not located within adipose tissue regions; that is, MCs originate from breast epithelial tissue. Thus, the VOI for the directed strategy consists of the set of all non-adipose phantom voxels. This VOI is convolved with the cluster rectangular hull to identify candidate insertion locations, as described above.

2.4 Simulation of mammographic projections

We simulated mammographic projections of the phantoms using a poly-energetic ray tracing method. Each voxel in the software phantom is associated with a linear attenuation coefficient, corresponding to the simulated tissue type. The voxels corresponding to inserted MCs were simulated as an admixture of calcified material and the background phantom tissue, with the linear attenuation coefficient given by:

$$\mu'(f,c) = f\mu_c c + (1-f)\mu_p \quad (1)$$

where μ' is the linear attenuation coefficient for a voxel in a phantom with a MC cluster; f is the fraction of the voxel volume occupied by the calcified tissue ($0<f<1$); μ_c is the linear attenuation coefficient of calcium hydroxyapatite; c is a parameter controlling the contrast of MCs in synthetic images ($0<c<1$); and μ_p is the linear attenuation coefficient of the phantom voxel before insertion. The resulting images were post-processed using a commercial image processing software package (Adara, Real Time Tomography, Villanova, PA) and saved in DICOM format.

2.5 Human observer study

We designed a 2-AFC observer study to validate the MC insertion method and compare the MC placement strategies. Images were created with both the directed and undirected placement strategies for every phantom-cluster pair from a set of phantoms and MC clusters. The observers were then required to select between images of the phantom produced with the two placement strategies.

Using a small pilot study (with one radiologist and 80 image pairs), we estimated that 450 image pairs were needed for the desired statistical power (Type II error < 0.05 with a Type I error of 0.05, resulting in an actual probability of a radiologist preferring direct placement in less than 42% of trials). To that end, we created 33 phantoms and selected 16 clusters from the database. The phantoms simulated a 450 ml breast with a thickness of 5 cm when compressed. Three sets of 11 phantoms each were created, with 15%, 20% and 30% volumetric glandularity, respectively. The clusters were selected based upon the number of individual MCs, and the spatial extent of the cluster. The number of MC in a cluster varied from 5 to 16. The cluster volume ranged from 0.008 to 9.328 mm^3. Among the 16 selected clusters, 10 were benign and six were malignant based on the pathology reports.

The image pairs for the 2-AFC study were generated by combining an image from each placement strategy for a given phantom-cluster pair. The left-right ordering of images, as well as the sequence of phantom-cluster pairs were randomized to avoid observer bias. Images were displayed using ViewDex (ver. 1.0_03; Sahlgrenska University Hospital and University of Gothenburg, Sweden) (20).

Each observer was instructed to select one image per pair based upon the plausibility of the cluster location in the phantom volume. For each image-pair shown, the observer was asked to answer four questions (see Fig. 4): (1) the visibility of the simulated cluster (in case of a negative answer, the remaining questions for the same image-pair were not considered for analysis); (2) the cluster realism (rated by five descriptive categories); (3) the preferred image of the pair; and (4) the confidence of the indicated preference (rated by a five category scale). The observer was instructed to select zero confidence if the observer had no preference between the images. The software recorded the answers along with elapsed time per image pair.

Three observers (all breast imaging fellows) participated in the 2-AFC study. During the study, we encouraged the observers to describe the rationale behind their preference, in terms of the MC cluster shape and location. The observer comments were recorded and matched with the appearance of simulated images.

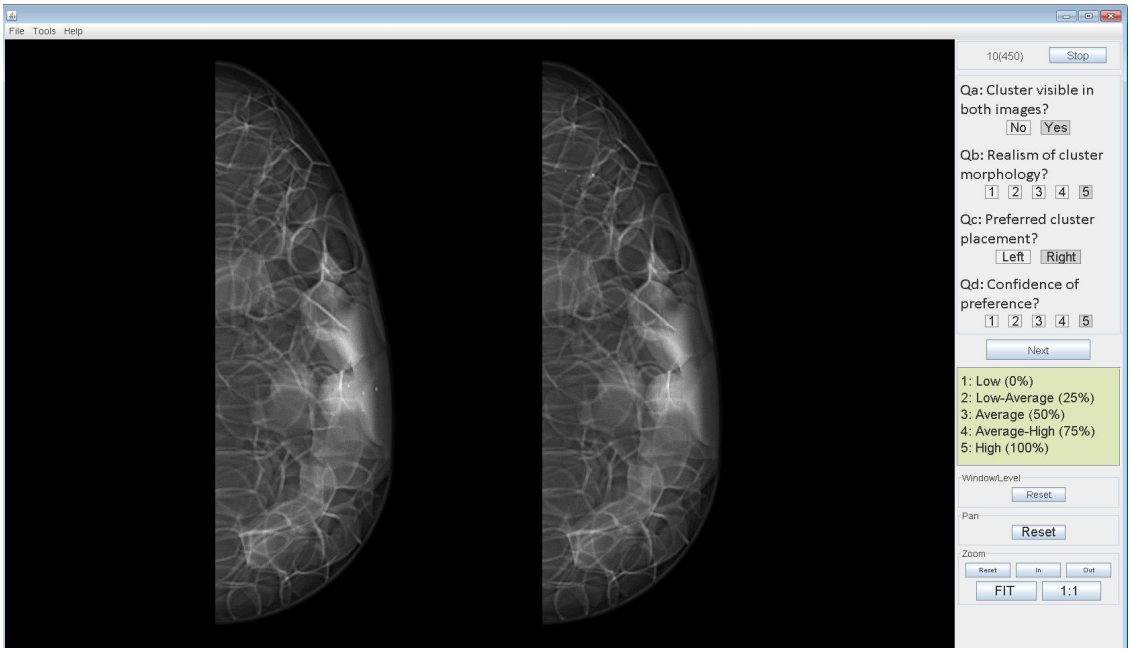

Figure 4: The 2-AFC observer study user interface, with an image pair and corresponding questions.

2.6 Statistical analysis

The observation data was analyzed as follows. Assume that a human observer is given a pair of images and with unknown probability p chooses a particular image. Let X=1 if the image with directed placement is chosen, and otherwise let X=0. The observer is provided a total of N image pairs. The random variable $Y = \sum_{i=1}^{N} X_i$ has a Binomial distribution with parameters N and p. Under the null-hypothesis, H_0, the observer does not have a preference between the directed and undirected strategies and p=0.5. To test H_0 vs. H_a (that the observer prefers undirected placement, p<0.5), we count the number of times, n, the observer chooses the directed placement. The p-value of the statistical test is computed as:

$$\text{p-value} = \sum_{i=0}^{n} \binom{N}{i} 0.5^i \, 0.5^{N-i} \tag{2}$$

We have also analyzed the dependence of the observers' preference on several factors, including the self-reported cluster realism level, the observer's confidence about the preference, the composition of the phantom at the location of cluster insertion, as well as the cluster location within the phantom.

3. RESULTS

3.1 Sections and projections of phantom with inserted MC clusters

Examples of the directed and undirected placement of MC clusters are shown in Figs. 5 and 6. Figure 5 shows the phantom and cluster in a single cross-section selected from the 3D volume. Figure 6 are projection images of the cluster after processing. These are typical of the images presented to the observers. We have added magnified regions of interest to aid in the review of the images for readers of this paper.

3.2 Observer study results

Overall preference of the directed cluster placement, calculated individually for each observer, as well as for all three observers combined, is shown in Table 1. The tabulated results indicate that the most of the clusters (93%) were visible. All the observers statistically significantly preferred the undirected placement strategy.

The observer's preference for insertion methods were further analyzed as a function of the confidence of their answers and cluster realism. The results are tabulated in Tables 2 and 3.

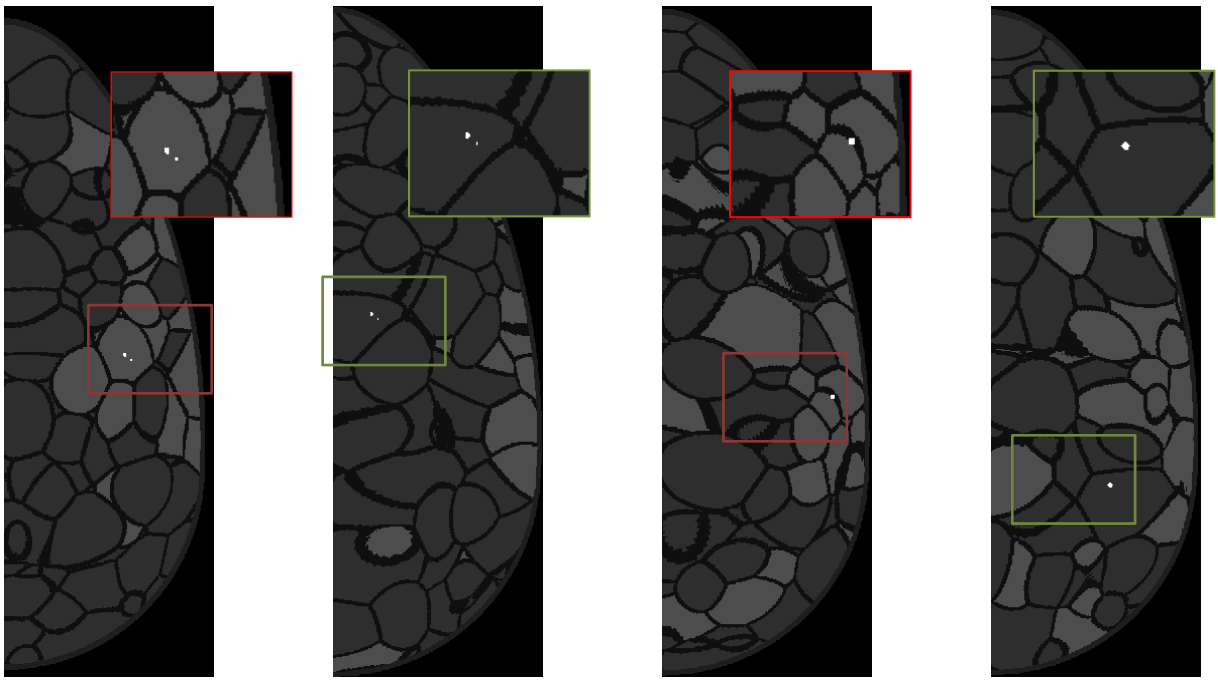

(a) (b) (c) (d)

Figure 5: Phantom slices illustrating two MC placement strategies. Enlarged are regions with inserted MCs. (a) A phantom with 15% glandularity, and directed placement; (b) the same phantom with undirected placement; (c) A phantom with 30% glandularity and directed placement; (d) the same phantom with undirected placement.

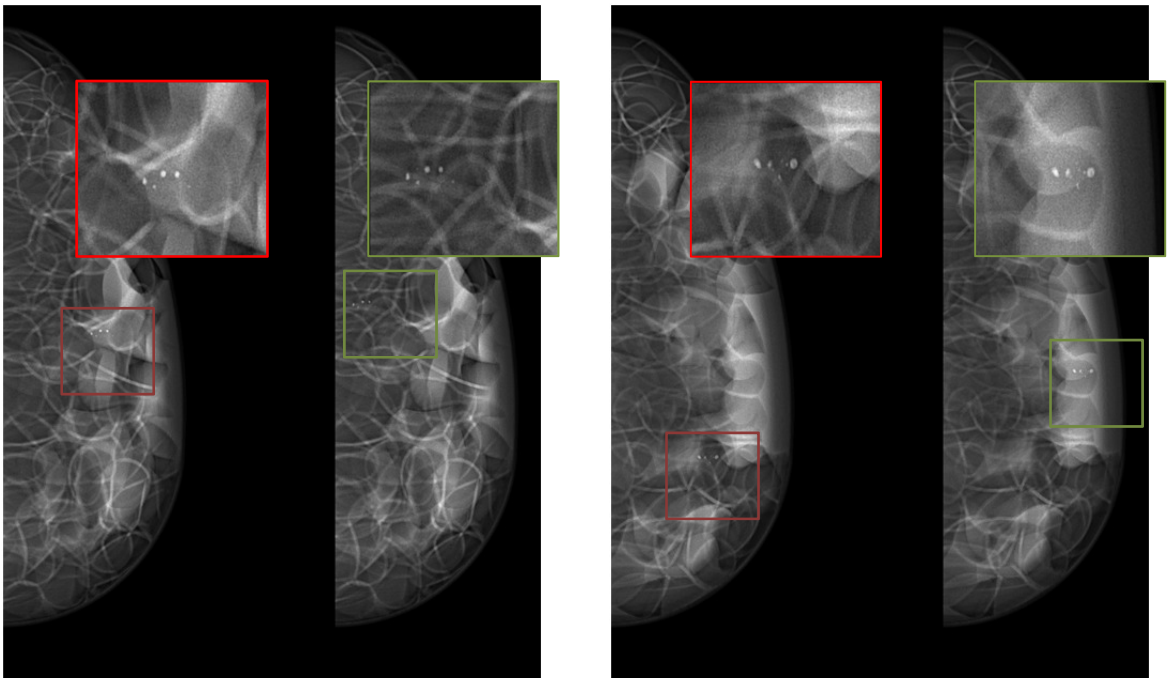

(a) (b)

Figure 6: Typical image pairs used in the validation study. Shown are synthetic mammographic projections corresponding to the phantoms from Fig. 5. Enlarged are regions with inserted MCs.

Table 1: Observer preference for the directed placement strategy.

Observer	Visible MCs (% of total)	Pref. directed (% of visible)	p-value
1	419 (93.11%)	169 (40.33%)	**4×10^{-5}**
2	416 (92.44%)	104 (25%)	**2×10^{-25}**
3	416 (92.44%)	136 (32.69%)	**7×10^{-13}**
All	1251 (92.67%)	409 (32.69%)	**3×10^{-25}**

Table 2: Observer preference for the directed strategy shown as a function of cluster realism.

Realism	Low (0%)	Low/Aver (25%)	Aver (50%)	Aver/High (75%)	High (100)
Observer 1					
Visible MCs (% total)	0 (0%)	62 (15%)	124 (30%)	278 (42%)	55 (13%)
Pref. directed (% visible)	0 (0%)	27 (44%)	62 (50%)	65 (37%)	15 (27%)
p-value	n/a	0.19	0.54	**2×10^{-4}**	**5×10^{-4}**
Observer 2					
Visible MCs (% total)	0 (0%)	33 (8%)	83 (20%)	155 (37%)	145 (35%)
Pref. directed (% visible)	0 (0%)	5 (8%)	25 (30%)	37 (24%)	37 (26%)
p-value	n/a	**3×10^{-5}**	**2×10^{-4}**	**2×10^{-11}**	**1×10^{-9}**
Observer 3					
Visible MCs (% total)	0 (0%)	2 (0.5%)	52 (12%)	356 (86%)	6 (1%)
Pref. directed (% visible)	0 (0%)	1 (50%)	19 (37%)	116 (33%)	0 (0%)
p-value	n/a	0.75	**0.04**	**2×10^{-11}**	n/a
All Observers					
Visible MCs (% total)	0 (0%)	97 (8%)	259 (21%)	689 (55%)	206 (16%)
Pref. directed (% visible)	0 (0%)	33 (34%)	106 (41%)	218 (32%)	52 (26%)
p-value	n/a	**1×10^{-3}**	**2×10^{-3}**	**1×10^{-22}**	**3×10^{-13}**

Table 3: Observer preference for the directed strategy shown as a function of decision confidence.

Confidence	Low (0%)	Low/Aver (25%)	Aver (50%)	Aver/High (75%)	High (100)
Observer 1					
Visible MCs (% total)	41 (10%)	64 (15%)	72 (17%)	209 (50%)	33 (8%)
Pref. directed (% visible)	16 (39%)	32 (50%)	34 (47%)	77 (37%)	10 (30%)
p-value	0.10	0.55	0.36	**9×10^{-5}**	**0.02**
Observer 2					
Visible MCs (% total)	19 (5%)	93 (22%)	71 (17%)	152 (37%)	81 (19%)
Pref. directed (% visible)	9 (47%)	34 (37%)	26 (37%)	29 (19%)	6 (7%)
p-value	0.50	**6×10^{-3}**	**0.02**	**3×10^{-15}**	**1×10^{-16}**
Observer 3					
Visible MCs (% total)	88 (21%)	180 (43%)	133 (32%)	14 (3%)	1 (0.2%)
Pref. directed (% visible)	44 (50%)	53 (29%)	34 (26%)	5 (36%)	0 (0%)
p-value	0.54	**2×10^{-8}**	**7×10^{-9}**	0.21	0.5
All Observers					
Visible MCs (% total)	148 (12%)	337 (27%)	276 (22%)	375 (30%)	115 (9%)
Pref. directed (% visible)	69 (47%)	119 (35%)	94 (34%)	111 (30%)	16 (14%)
p-value	0.23	**4×10^{-8}**	**6×10^{-8}**	**8×10^{-16}**	**4×10^{-16}**

As stated elsewhere in the paper, in the directed strategy, clusters were always positioned on a background of non-adipose tissues. In the undirected strategy, however, the cluster could be positioned over adipose and non-adipose tissues. Table 4 shows the observers' preference as a function of composition of background tissues, calculated as the percentage of non-adipose tissue in regions of phantoms that correspond to the rectangular hull of the inserted cluster.

Table 4: Observer preference as a function of the background composition of the undirected MC clusters.

Phantom % dense @ insertion location	**Very dense**	**Predom. dense**	**Average**	**Predom. fat**	**Very fatty**
Observer 1					
Visible MCs	49	5	20	66	58
Pref. directed (% vis.)	23 (47%)	2 (40%)	8 (40%)	25 (38%)	18 (31%)
p-value	4×10^{-1}	5×10^{-1}	2×10^{-1}	$\mathbf{3 \times 10^{-2}}$	$\mathbf{3 \times 10^{-3}}$
Observer 2					
Visible MCs	48	5	20	67	57
Pref. directed (% vis.)	21 (44%)	1 (20%)	8 (40%)	16 (24%)	11 (19%)
p-value	2×10^{-1}	2×10^{-1}	2×10^{-1}	$\mathbf{1 \times 10^{-5}}$	$\mathbf{2 \times 10^{-6}}$
Observer 3					
Visible MCs	47	5	20	66	59
Pref. directed (% vis.)	20 (43%)	2 (40%)	11 (55%)	24 (36%)	17 (29%)
p-value	2×10^{-1}	5×10^{-1}	8×10^{-1}	$\mathbf{2 \times 10^{-2}}$	$\mathbf{8 \times 10^{-4}}$
All Observers					
Visible MCs	144	15	60	199	174
Pref. directed (% vis.)	64 (44%)	5 (33%)	27 (45%)	65 (33%)	46 (26%)
p-value	1×10^{-1}	$\mathbf{2 \times 10^{-3}}$	$\mathbf{3 \times 10^{-3}}$	$\mathbf{6 \times 10^{-7}}$	$\mathbf{2 \times 10^{-10}}$

Based upon the known MC insertion locations, we plotted the distribution of preferred vs. non-preferred cluster locations, for the directed placement strategy (see Fig. 7).

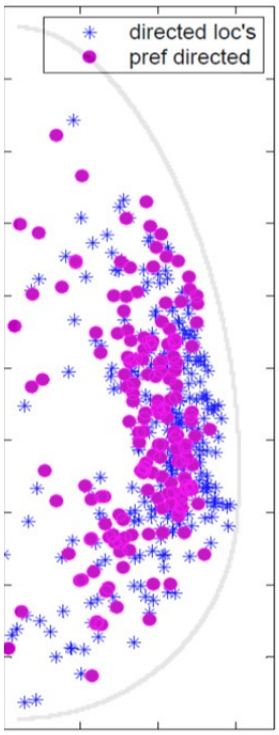

Figure 7: Graphical representation of the observer preference as a function of cluster location for one observer. The points mark the center location of each cluster placed according to the directed strategy for every image pair in study. The asterisk represent locations where the directed placement strategy placed MC clusters (but which were not preferred), and the circles represent locations were the directed points were preferred.

3.3 Observer comments

During the study, we recorded a number of insightful comments from observers about the appearance of simulated clusters and phantoms, and about the reasoning behind their preference for a specific image from an image pair. Several anecdotal comments are illustrated in Fig. 8.

"Very realistic, cluster with 2 punctuate and 1 indistinct calcification; pretty suspicious; less frequently seen this close to the nipple (referring to directed placement - left)"

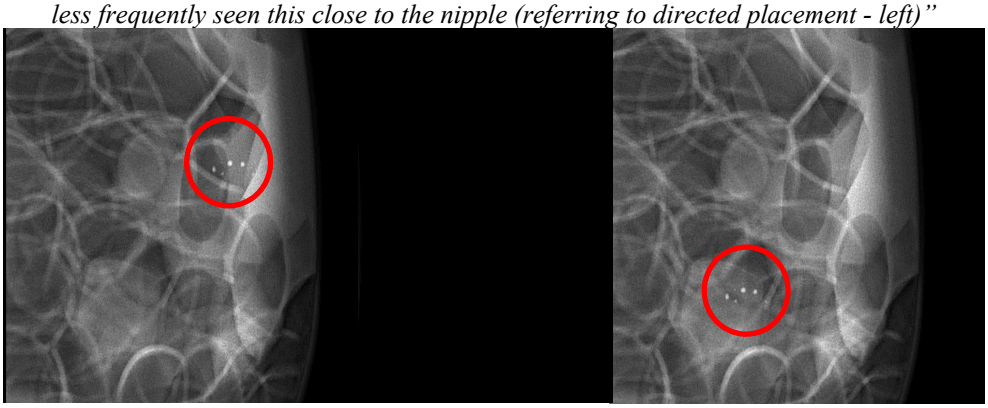

"The cluster looked too close to the skin; its appearance is similar to a fibroadenoma (with peripheral distribution on an oval shaped lesions). These lesions are rarely seen so close to the nipple; they are seen more frequently in the upper half (referring to directed placement - left)

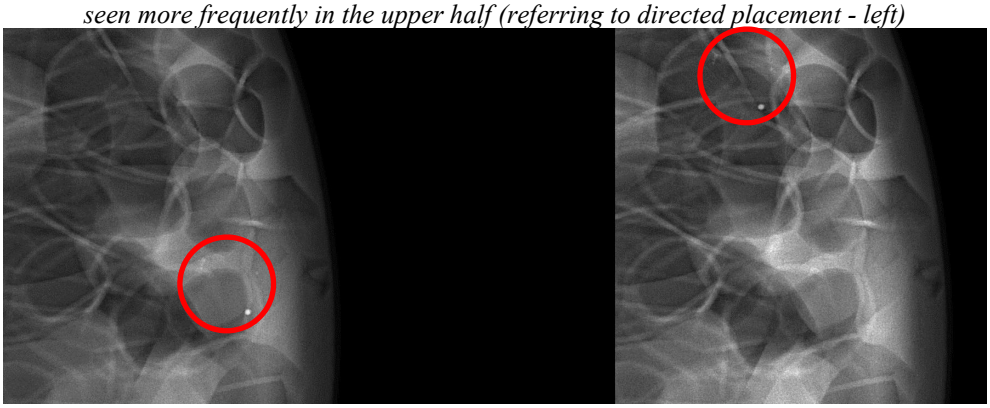

"Appearance of calcification with holes more typical for dermal regions and more plausible to be on posterior side (referring to undirected placement - right)"

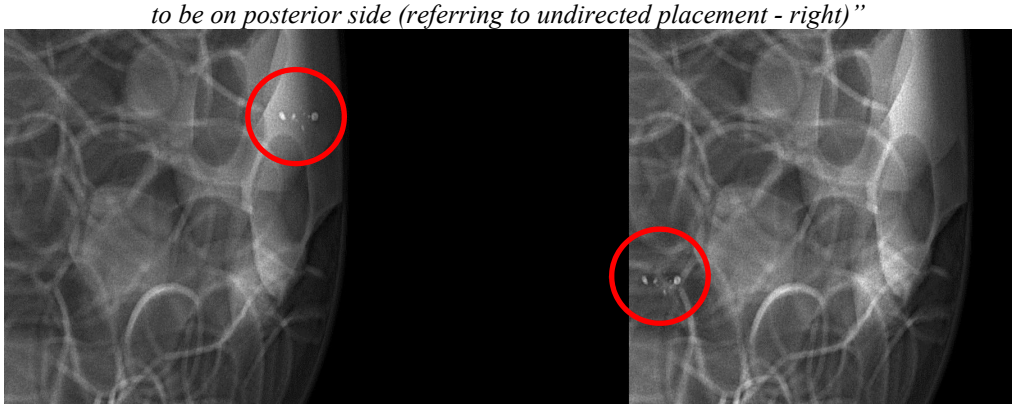

Figure 8: Synthetic image pairs in which radiologists commented upon the MC cluster. In these examples, the directed placement is on the left and the undirected placement is on the right. (Circles have been added to mark the cluster)

4. DISCUSSION

We have successfully implemented an automated method for insertion of simulated MC clusters into software breast phantoms, using two different placement strategies. A 2-AFC observer study with three radiologists has been used to validate the insertion method, and to identify the preferred placement strategy.

The analysis of cluster realism (Table 2) shows that the observers found that the simulated clusters have a high level of realism. In total, the observers found the cluster to be realistic (i.e., realism rated average or higher) in 92% of cases, validating the insertion method. This high level of realism supports our use of the automated insertion method. As such, it will now be fully incorporated and accelerated in our GPU-based VCT pipeline software.

The insertion method allows for the placement of MC clusters to be guided by a pdf. Two pdf were compared: a uniform pdf, and a pdf that placed MC clusters in fibroglandular tissue. The results of the preference study, summarized in Table 1, show that all observers statistically significantly preferred the undirected strategy. The directed strategy was preferred 33% of clusters, and undirected strategy was preferred in 67% of clusters. This indicates that the clusters did not look realistic on a background of glandular tissue.

Support for this premise is evident in Table 4, which shows the probability of selecting the directed strategy as a function of the background of the MC cluster in the image with undirected placement. These data do not show any preference for the placement strategy when the undirected placement strategy selected a MC cluster location within a dense tissue region. This result is sensible since the directed placement locations are, by definition, selected within dense tissue regions; thus, when both strategies select a dense background, the radiologists have no reason to prefer one strategy over the other.

Table 4 also shows that the preference for the placement of a cluster increases as the background composition at the insertion site becomes increasingly less dense. Thus, radiologists prefer clusters that are superimposed upon a predominantly adipose region. The observed preference may be due, in part, to the increased contrast of MCs in adipose regions. The adipose regions also have more visible simulated anatomical structures including prominent ligaments, potentially creating a set of features that aid in making diagnostic decisions about the detected cluster. As such, we plan to explore methods for adding structure in fibroglandular regions of our breast phantoms.

All the reported results from our observer study provide evidence that the undirected strategy produced more plausible simulations. It can be seen that as the observers' confidence increased (Table 3), the radiologists were more likely to prefer the undirected strategy. This evidence has led us to reject our original hypothesis about modeling MCs exclusively in dense phantom regions, which we justified by considering the epithelial origins of breast calcifications. Calcifications do originate from epithelial tissue histologically; however, it is now clear that we should not restrict potential MC cluster locations exclusively to dense mammographic regions.

An additional contributing factor may be that we currently simulate dense tissue regions as having a uniform composition within the interior of dense compartments. Thus, the glandular tissue may lack realism. We have previously tested other methods for simulating glandular tissue, including the use of subcompartments, (21) adding filtered binarized noise, (22, 23) or Perlin noise (24). As future work, we will test cluster realism with these various glandular tissue simulation methods.

Finally, Fig. 7 showed the preferred locations of MC clusters. It is clear that radiologists do not prefer MC clusters that are located near the distal edge of the breast. This finding is also supported by observers' comments, which not only prefer posterior locations, but also suggest that cluster location can lead to different interpretations of pathology. We plan to analyze observer preference as a function of cluster location, and intend to revise the placement strategy to improve realism further, if possible.

5. CONCLUSIONS

We have developed an automatic method to insert microcalcifications into software breast phantoms. This method was developed to help support VCTs that require large numbers of simulated breasts. We validated the insertion method in a 2-AFC study with radiologist observers. The radiologists found the resulting cluster placement to be realistic in 92% of cases. The insertion method allows for the placement of MC clusters to be guided by a probability density function. There was a significant preference for the cluster to be positioned on a background of adipose or mixed adipose/fibroglandular tissues. These results support our inclusion of this automated placement algorithm into our

simulation pipeline. Given that there was a strong preference for certain cluster locations, further research will be performed to continue to improve realism.

ACKNOWLEDGMENT

This work was supported in part by the US National Institutes of Health (R01 grant #CA154444), the US Department of Defense Breast Cancer Research Program (HBCU Partnership Training Award #BC083639), the US National Science Foundation (CREST grant #HRD-0630388 and III grant # 0916690), and the US Department of Defense/Department of Army (45395-MA-ISP, #54412-CI-ISP, W911NF-11-2-0046). The content is solely the responsibility of the authors and does not necessarily represent the official views of the NIH, NSF or DoD. The authors are thankful to Ms. Susan Ng from Real-Time Tomography (Villanova, PA) for processing the simulated projection images.

REFERENCES

1. Bakic PR, Albert M, Brzakovic D, Maidment ADA. Mammogram synthesis using a 3D simulation. II. Evaluation of synthetic mammogram texture. Medical Physics. 2002;29(9):2140-51.
2. Bakic PR, Albert M, Brzakovic D, Maidment ADA. Mammogram synthesis using a 3D simulation. I. Breast tissue model and image acquisition simulation. Medical Physics. 2002;29(9):2131-9.
3. Bakic PR, Zhang C, Maidment ADA. Development and Characterization of an Anthropomorphic Breast Software Phantom Based upon Region-Growing Algorithm. Medical Physics. 2011;38(6):3165-76.
4. Pokrajac DD, Maidment ADA, Bakic PR. Optimized generation of high resolution breast anthropomorphic software phantoms. Medical Physics. 2012;39(4):2290-302.
5. Bliznakova K, Suryanarayanan S, Karellas A, Paiilikarakis N. Evaluation of an improved algorithm for producing realistic 3D breast software phantoms: Application for mammography. Medical Physics. 2010;37(11):5604-17.
6. Li CM, Segars WP, Tourassi GD, Boone JM, Dobbins III JT. Methodology for generating a 3D computerized breast phantom from empirical data. Medical Physics. 2009;36(7):3122-31.
7. Chen B, Shorey J, Saunders RSJ, Richard S, Thompson J, Nolte LW, et al. An anthropomorphic breast model for breast imaging simulation and optimization. Academic Radiology. 2011;18(5):536-46.
8. O'Connor JM, Das M, Didier CS, Mahd M, Glick SJ. Generation of voxelized breast phantoms from surgical mastectomy specimens Medical Physics. 2013;40(4):041915.
9. Hoeschen C, Fill U, Zankl M, Panzer W, Regulla D, Dohring W. A high resolution voxel phantom of the breast for dose calculations in mammography. Radiation Protection Dosimetry 2005;114(1-3):406-9.
10. Shaheen E, Van Ongeval C, Cockmartin L, Zanca F, Marshall NW, Jacobs J, et al. Realistic Simulation of Microcalcifications in Breast Tomosynthesis. In: Marti Jea, editor. International Workshop on Digital Mammography (IWDM); Girona, Spain: Springer; 2010. p. 235-42.
11. Lefebvre F, Benali H, Gilles R, Di Paola R. A simulation model of clustered breast microcalcifications. Medical Physics. 1994;21(12):1865-74.
12. Warren LM, Green FH, Shrestha L, Mackenzie A, Dance DR, Young KC. Validation of simulation of calcifications for observer studies in digital mammography. Physics in Medicine and Biology. 2013;58:N217-N28.
13. Maidment ADA, Albert M, Conant EF. Three-dimensional imaging of breast calcifications. In: Selander JM, editor. 26th AIPR Workshop: Exploiting New Image Sources and Sensors; 1998; Washington, D.C.: SPIE; 1998. p. 200-8.
14. Maidment ADA, Albert M, Feig SA. 3-D Mammary Calcification Reconstruction from a Limited Number of Views. Physics of Medical Imaging; 1996; San Diego: SPIE; 1996. p. 378-89.
15. Chui JH, Zeng R, Pokrajac DD, Park S, Myers KJ, Maidment ADA, et al. Two methods for simulation of dense tissue distribution in software breast phantoms. Physics of Medical Imaging; lake Buena Vista, FL: SPIE; 2013.
16. Ruiter NV, Zhang C, Bakic PR, Carton A-K, Kuo J, Maidment ADA. Simulation of tomosynthesis images based on an anthropomorphic software breast tissue phantom. In: Miga MI, Cleary KR, editors. SPIE Medical Imaging: Visualization, Image-guided Procedures, and Modeling San Diego, CA2008.
17. Xia S, Liu F, Maidment ADA, Bakic PR. Refinements to the Deformation Model of an Anthropomorphic Computer Generated Breast Phantom. Medical Physics. 2010;37:3131.
18. Lago MA, Maidment ADA, Bakic PR. Modelling of mammographic compression of anthropomorphic software breast phantom using FEBio. Int'l Symposium on Computer Methods in Biomechanics and Biomedical Engineering; Salt Lake City, UT2013.
19. Kuo J, Ringer P, Fallows SG, Ng S, Bakic PR, Maidment ADA, editors. Dynamic reconstruction and rendering of 3D tomosynthesis images. Physics of Medical Imaging; 2011; Lake Buena Vista, FL: SPIE.

20. Hakansson M, Svensson S, Zachrisson S, Svalkvist A, Bath M, Mansson LG. ViewDEX: an efficient and easy-to-use software for observer performance studies. Radiation Protection Dosimetry. 2010;139:42-50.
21. Abbey CK, Bakic PR, Pokrajac DD, Maidment ADA, Eckstein MP, Boone JM. Non-Gaussian Statistical Properties of Virtual Breast Phantoms. In: Mello-Thoms CR, Kupinski MA, editors. SPIE Image Perception, Observer Performance, and Technology Assessment; San Diego, CA: SPIE; 2014.
22. Reiser I, Lau AB, Nishikawa RM, Bakic PR. A directional small-scale tissue model for an anthropomorphic breast phantom. International Workshop on Breast Imaging; Philadelphia, PA: Springer; 2012.
23. Lau AB, Reiser I, Nishikawa RM, Bakic PR. A statistically defined anthropomorphic software breast phantom Medical Physics. 2012;39(6):3375-85.
24. Timberg P. Technical optimisation of digital breast tomosynthesis for future breast screening. European Congres of Radiology; Vienna, Austria2014.